Aerosol particles at a high-altitude site on the Southeast Tibetan Plateau, China: Implications for pollution transport from South Asia

Zhuzi Zhao,[1] Junji Cao,[1] Zhenxing Shen,[2] Baiqing Xu,[3] Chongshu Zhu,[1] L.-W. Antony Chen,[4] Xiaoli Su,[1] Suixin Liu,[1] Yongming Han,[1] Gehui Wang,[1] and Kinfai Ho [1,5]

Received 30 October 2012; revised 16 May 2013; accepted 23 June 2013; published 4 October 2013.

[1] Bulk aerosol samples were collected from 16 July 2008 to 26 July 2009 at Lulang, a high-altitude (>3300m above sea level) site on the southeast Tibetan Plateau (TP); objectives were to determine chemical characteristics of the aerosol and identify its major sources. We report aerosol (total suspended particulate, TSP) mass levels and the concentrations of selected elements, carbonaceous species, and water-soluble inorganic ions. Significant buildup of aerosol mass and chemical species (organic carbon, element carbon, nitrate, and sulfate) occurred during the premonsoon, while lower concentrations were observed during the monsoon. Seasonal variations in aerosol and chemical species were driven by precipitation scavenging and atmospheric circulation. Two kinds of high-aerosol episodes were observed: one was enriched with dust indicators (Fe and Ca^{2+}), and the other was enhanced with organic and elemental carbon (OC and EC), SO_4^{2-}, NO_3^-, and Fe. The TSP loadings during the latter were 3 to 6 times those on normal days. The greatest aerosol optical depths (National Centers for Environmental Protection/National Center for Atmospheric Research reanalysis) occurred upwind, in eastern India and Bangladesh, and trajectory analysis indicates that air pollutants were transported from the southwest. Northwesterly winds brought high levels of natural emissions (Fe, Ca^{2+}) and low levels of pollutants (SO_4^{2-}, NO_3^-, K^+, and EC); this was consistent with high aerosol optical depths over the western deserts and Gobi. Our work provides evidence that both geological and pollution aerosols from surrounding regions impact the aerosol population of the TP.

Citation: Zhao, Z., et al. (2013), Aerosol particles at a high-altitude site on the Southeast Tibetan Plateau, China: Implications for pollution transport from South Asia, *J. Geophys. Res. Atmos.*, *118*, 11,360–11,375, doi:10.1002/jgrd.50599.

1. Introduction

[2] The Tibetan Plateau (TP), the world's highest and largest plateau, exerts a major influence on the monsoonal circulation in Asia [*An et al.*, 2001]. Moreover, the TP not only affects large-scale atmospheric circulation, but it also impacts the hydrological cycle of the entire Asian continent. These effects are mediated through its dynamical and thermal influences on the atmosphere as well as through snow and glacier melt [*Lau et al.*, 2010; *Wu et al.*, 2007].

[3] The TP is at the juncture of several important natural and anthropogenic aerosol sources, including the Taklimakan and Gobi Desert to the north and northwest, deserts in southwestern Asia and the Middle East to the west and southwest, densely populated areas in the Indo-Gangetic Plain, and areas in South Asia where biomass is burned extensively [*Xia et al.*, 2011]. Transport of pollutants from the densely populated countries (such as India, Pakistan, China, and Nepal) to the Himalayas may not only result in substantial radiative forcing in South Asia with potential effects on the monsoon circulation but also on regional climate and hydrological cycles [*Venzac et al.*, 2008]. Black carbon (BC) that is deposited on the TP absorbs solar radiation, and it is one of the most important substances that cause the melting of ice and snow. Recent studies show that over the past decade, Tibetan glaciers have been melting at an accelerating rate, raising the threat of future shortages in the water supply in neighboring countries [*Xu et al.*, 2009].

[4] High-elevation sites are well suited for sampling the free troposphere, and studies at those sites are particularly useful for characterizing typical background conditions and

[1]Key Lab of Aerosol Science and Technology, SKLLQG, Institute of Earth Environment, Chinese Academy of Sciences, Xi'an, China.
[2]Department of Environmental Science and Engineering, Xi'an Jiaotong University, Xi'an, China.
[3]Laboratory of Tibetan Environment Changes and Land Surface Processes, Institute of Tibetan Plateau, Chinese Academy of Science, Beijing, China.
[4]Division of Atmospheric Sciences, Desert Research Institute, Reno, Nevada, USA.
[5]School of Public Health and Primary Care, Chinese University of Hong Kong, Hong Kong, China.

Corresponding author: J. Cao, Key Lab of Aerosol Science and Technology, SKLLQG, Institute of Earth Environment, Chinese Academy of Sciences, Xi'an 100085, China. (jjcao@ieecas.cn)

2169-897X/13/10.1002/jgrd.50599

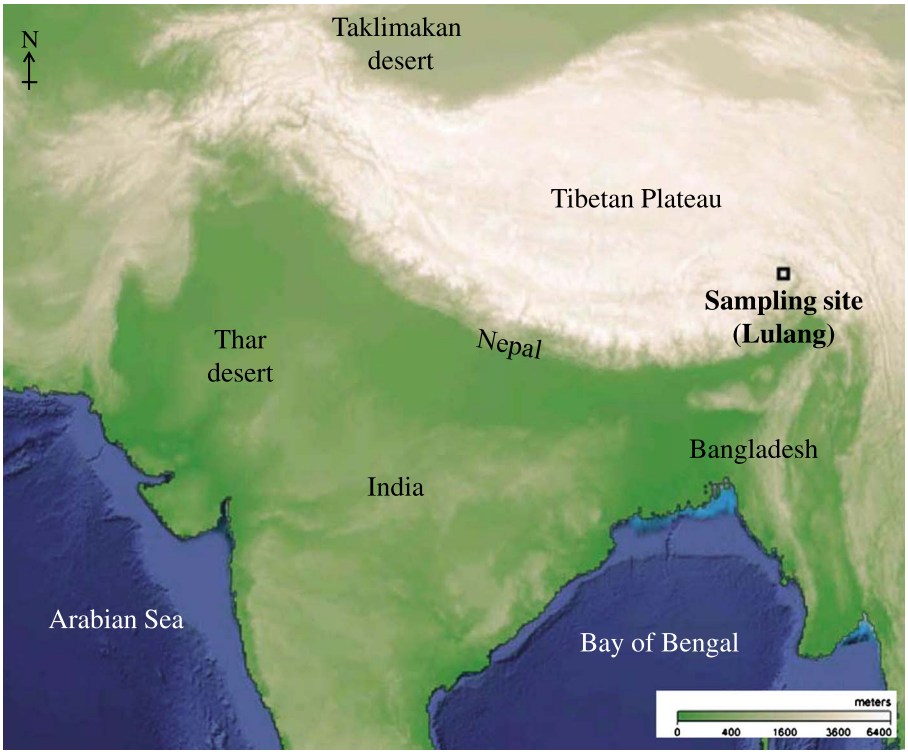

Figure 1. Geographical location of the sampling site. Adapted from www.earthobservatory.nasa.gov.

investigating the influences of human activity on its composition. In the past decade, numerous scientific studies have been conducted in the Indo-Asia-Pacific region, and an extensive observational system has been developed within the Indian Ocean Experiment project [*Ramanathan and Crutzen*, 2003]. Studies at these sites have served to better understand the "brown cloud" which can extend from the Indian Ocean to the Himalayan range, attain a vertical thickness of about 3 km [*Ramanathan et al*., 2007] during the dry season (especially from November to March), and affect some of the most populous Asian regions, currently home of more than 2 billion persons.

[5] Atmospheric aerosols build up over the southern slope of the TP during the premonsoon season, and they are lifted by the Himalayan topography [*Xia et al*., 2011]. Aerosol mass and BC concentrations increased significantly over the southeastern TP during a dry period when numerous fires burned, and there was transport of pollution from nearby regions in South Asia and the northern part of the Indian Peninsula [*Engling et al*., 2011]. Some previous investigators have already suggested that the southern Himalayas are affected by significant amounts of pollution that is either uplifted by the typical valley circulation or advected by regional and long-range transport events [*Hindman and Upadhyay*, 2002; *Bonasoni et al*., 2008]. Observations at the Nepal Climate Observatory-Pyramid provide convincing evidence that the southern side of the high Himalayan valleys represents a "direct channel" through which brown cloud pollutants can be transported up to 5 km above sea level (asl) especially during the premonsoon period; this is a case where normally clean atmospheric conditions could be strongly compromised [*Bonasoni et al*., 2010]. However, the effects of the Tibetan aerosol on regional climate variability remain largely unknown, and this is due, at least in part, to the limited number of observations over the plateau.

[6] Although the monitoring of atmospheric composition at high altitudes is recognized as important for understanding climate change, experimental work in high-altitude regions has been sparse [*Carrico et al*., 2003; *Hindman and Upadhyay*, 2002]. To this end, we conducted a 1 year study of bulk aerosol (total suspended particulate, TSP) at Lulang, which is on the southeastern flank of the TP. The study focused on selected aerosol chemical components, including organic (OC), elemental carbon (EC), water-soluble inorganic ions, and dust-derived trace elements, and it included an assessment of their seasonal variability, especially in relation to the monsoonal circulation. We show how anthropogenic activities dramatically perturb the background aerosol levels and discuss how the aerosol chemical composition changes in such cases (episodes). Potential sources for the aerosol particles and their transport pathways during high-aerosol loading episodes are also evaluated and discussed.

2. Data and Methodology

2.1. Aerosol Sampling

[7] The Lulang sampling site (Figure 1) is situated in Linzhi Prefecture, which is on the southeastern margin of the TP (94.44°E, 29.46°N). To the west of the sampling site is the Yarlung Tsangpo River Valley, which has an altitude of 3300 m, and the Himalaya Mountains rise south of the site. Lulang is approximately 30 to 50 km west of several

Table 1. Seasonal Meteorological Characteristics at Lulang

Season	Start Date (YYYY-MM-DD)	End Date (YYYY-MM-DD)	Surface Pressure (hPa)	Relative Humidity (%)	Daily Mean Temperature (°C)	Total Precipitation (mm)	Average Wind Speed ($m\,s^{-1}$)
2008 M[a]	2008-07-16	2008-10-03	681.94	82.65	11.63	340.80	1.47
Post-M[b]	2008-10-04	2008-11-09	684.90	72.67	3.37	82.80	1.57
Winter	2008-11-10	2009-02-17	681.66	64.98	−1.77	6.60	1.72
Pre-M[c]	2009-02-18	2009-04-27	679.70	71.39	2.73	98.60	1.93
2009 M[d]	2009-04-28	2009-07-26	680.54	76.78	11.05	296.00	1.70
Annual	2008-07-16	2009-07-26	681.40	73.51	5.50	824.80	1.69

[a]Monsoon in 2008.
[b]Postmonsoon.
[c]Premonsoon.
[d]Monsoon in 2009.

small villages [*Cao et al*., 2010]. There are extensive forests in Linzhi, and the sampling site is located in a remote area with no major anthropogenic sources nearby. Hence, long-range transport from upwind regions to the plateau is the presumptive cause for elevated pollutant concentrations. During the summer monsoon, low-pressure systems over the plateau induce a flow of moist warm air from the Indian and Pacific Oceans to the Indian subcontinent and TP. In winter, on the other hand, high-pressure systems drive cold, dry air out of the plateau [*Byson*, 1986; *Tang*, 1998].

[8] Sampling was normally conducted once every 6 days starting at 10:30 Beijing Time (BJT), and the sampling intervals were typically 3 days. Aerosol (TSP) samples were collected at a flow rate of 40 L/min with a KC-120H QingDao Laoshan sampler (Laoshan Electronic Instrument Factory Co., LTD., QingDao, China). The flow rate of the sampler was lowered from 100 L/min to 40 L/min to adjust for the atmospheric pressure in this high-altitude site. The aerosol particles were collected on 90 mm Whatman quartz fiber filters (QM-A™, Whatman, Clifton, NJ, USA) from 16 July 2008 to 26 July 2009. The filters were preconditioned by heating at 900°C for 3 h to remove residual carbon. After sampling, the filters were transported in a portable cooler to the aerosol laboratory at the Institute of Earth Environment, Chinese Academy of Sciences, to avoid the loss of volatile compounds. Field blank filters were also collected periodically by exposing filters in the sampler without drawing air through them; these were used to account for any artifacts introduced during the sample handling process.

[9] An automatic weather station was installed at the sampling site, and meteorological data, including wind speed and direction, air temperature, precipitation, air pressure, and relative humidity, were collected routinely. Abrupt variations in relative humidity (RH), wind direction (WD), and precipitation were used to identify the onset and conclusion of the summer monsoon and winter seasons. Based on the seasonality of atmospheric circulation, the annual cycle was defined as follows: monsoon (16 July 2008 to 3 October 2008; 28 April 2009 to 26 July 2009), postmonsoon (4 October 2008 to 9 November 2008), winter season (10 November 2008 to 17 February 2009), and premonsoon (18 February 2009 to 30 April 2009). Table 1 summarizes the meteorological conditions during the study. A total of 61 samples were collected; 27 of these were collected during the monsoon, 6 during the postmonsoon, 16 during the winter season, and 12 during the premonsoon.

2.2. Experimental

2.2.1. Gravimetric Analysis

[10] After ~24 h equilibration at a temperature between 20 and 23°C and RH between 35 and 45%, the quartz fiber filters were analyzed gravimetrically for mass concentrations with the use of a Sartorius MC5 electronic microbalance that had a sensitivity of ±1 μg (Sartorius, Göttingen, Germany). Each filter was weighed at least three times before and after sampling, and the net mass accumulation was obtained by subtracting the difference between the averaged presampling and postsampling weights.

2.2.2. Water-Soluble Inorganic Ions Analysis

[11] An aliquot of a sample filter (~4.33 cm^2) was extracted with 10 mL of ultrapure water for the inorganic ion studies. Eight inorganic ion concentrations (Na^+, NH_4^+, K^+, Mg^{2+}, Ca^{2+}, Cl^-, NO_3^-, and SO_4^{2-}) were determined with the use of a DX600 ion chromatography system (Dionex Inc., Sunnyvale, CA, USA). A CS12 column (150 × 4 mm) and an AS14 column (150 × 4 mm) were used for cation and anion analysis, respectively. Standard reference materials produced by the National Research Center for Certified Reference Materials (Beijing, China) were analyzed for quality control and assurance purposes [*Zhang et al.*, 2011]. Field blank levels were averaged and subtracted from the samples. Ten percent of the samples were submitted for replicate analyses, yielding coefficients of variance of ±0.25% for Na^+, ±22.8% for NH_4^+, ±1.82% for K^+, ±2.90% for Mg^{2+}, ±3.75% for Ca^{2+}, ±1.59% for Cl^-, ±2.34% for NO_3^-, and ±1.39% for SO_4^{2-}.

2.2.3. OC and EC Analysis

[12] A 0.5 cm^2 punch from each quartz filter was analyzed for OC and EC by the IMPROVE_A thermal/optical reflectance protocol [*Chow et al*., 2007] and the use of a Desert Research Institute (Reno, NV, USA) Model 2001 thermal/optical carbon analyzer (Atmoslytic Inc., Calabasas, CA, USA). Details of the method, including quality assurance/quality control (QA/QC) procedures, are described in *Cao et al*. [2003].

2.2.4. Elemental Analysis

[13] All samples were analyzed by energy dispersive X-ray fluorescence spectrometry with the use of an Epsilon 5 XRF analyzer (PANalytical, Almelo, Netherlands). The X-ray source was a side window X-ray tube with a gadolinium anode; the instrument operated at an acceleration voltage between 25 and 100 kV and a current of 0.5 to 24 mA (maximum power: 600 W). The characteristic X-ray radiation was detected with the use of a PAN 32 germanium detector.

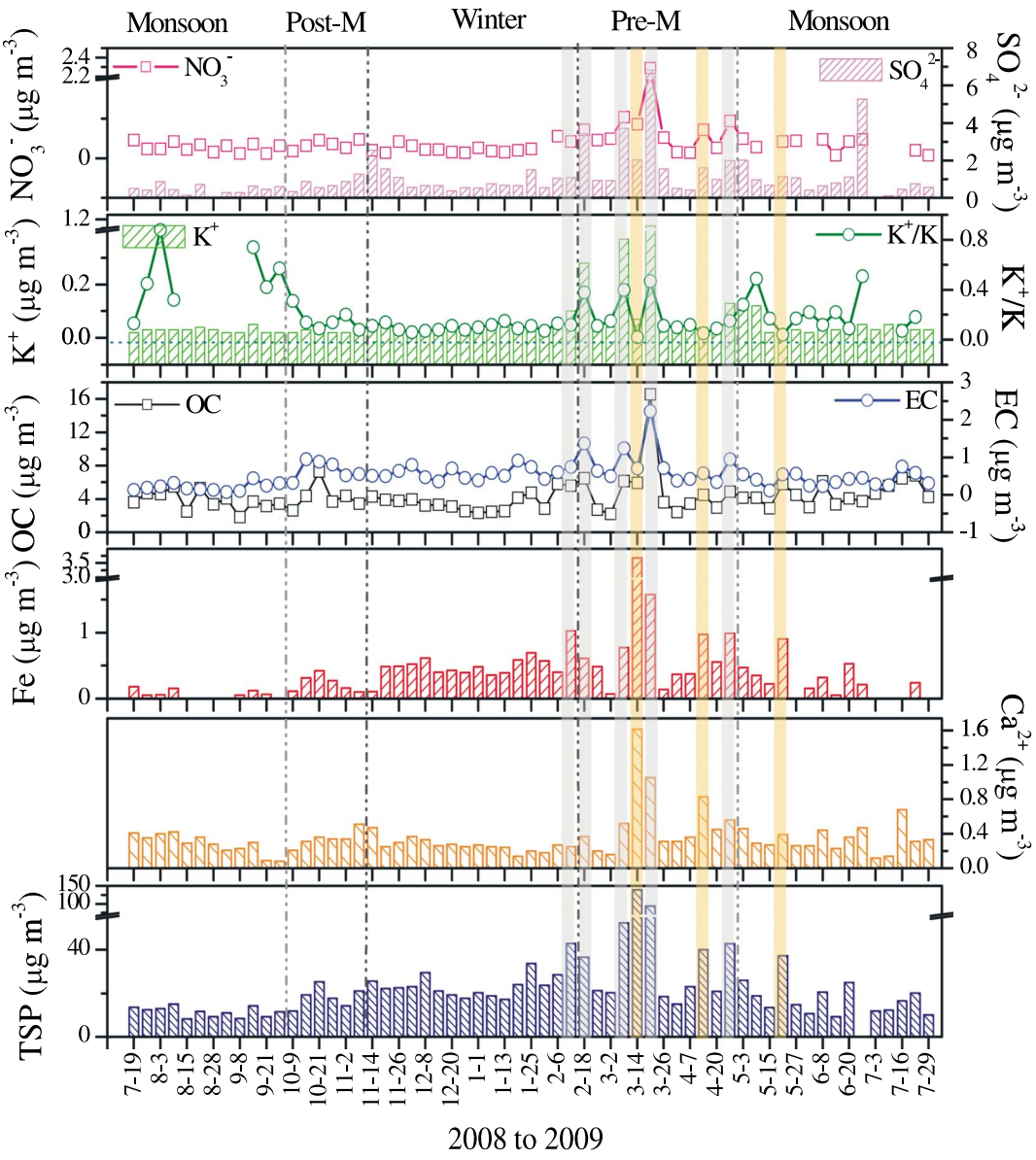

Figure 2. Temporal variations of analyzed chemical species in total suspended particle (TSP) samples from Lulang (July 2008 to July 2009) (yellow: episode type I; gray: episode type II).

[14] Concerns over the validity of the elemental data for the quartz fiber filters led to an intercomparison of elemental concentrations for samples collected on two different types of filters. The intercomparison study was based on XRF measurements made on nine collocated Teflon-membrane and quartz fiber filters from Xi'an. The concentrations were found to be comparable, with correlations (r) ranging from 0.982 for Fe and Zn (slopes of 1.054 and 1.062, respectively) to 0.915 for As (slope of 1.204) for these elements. Measurement precision was calculated as the standard deviation of several analyses of the same sample; the precisions were ±7.6% for Fe, ±8.6% for Ti, ±12.5% for Mn, ±7.6% for Zn, ±23.5% for As, ±33.3% for Br, and ±7.9% for Pb at typical concentration levels [*Cao et al.*, 2012]. The QA/QC of the analysis is described by Xu [*Xu et al.*, 2012].

[15] In this study, Fe and K were used to estimate the loadings of crustal matter and to evaluate the influence of biomass burning, respectively. Prior studies have shown that Fe accounts for 4% of Asian dust and Chinese loess [*Zhang et al.*, 2003]; hence, soil dust concentrations were estimated from the following equation:

$$C_{\text{soil dust}} = C_{\text{Fe}}/4\% \quad (1)$$

where $C_{\text{soil dust}}$ is soil dust concentration and C_{Fe} is the elemental Fe concentration. And K^+/K ratio was used to evaluate the extent of biomass burning or dust in different episodes [*Shen et al.*, 2007]. Moreover, S, K, Fe, Ca, and Ti were used for source apportionments by positive matrix factorization (PMF).

2.3. Satellite Data

[16] Space-based sensors provide near-real-time information on atmospheric aerosols, and the data obtained with them are invaluable because the coverage is global and spatial resolution kilometer scale [*King et al.*, 1999; *Kaufman*

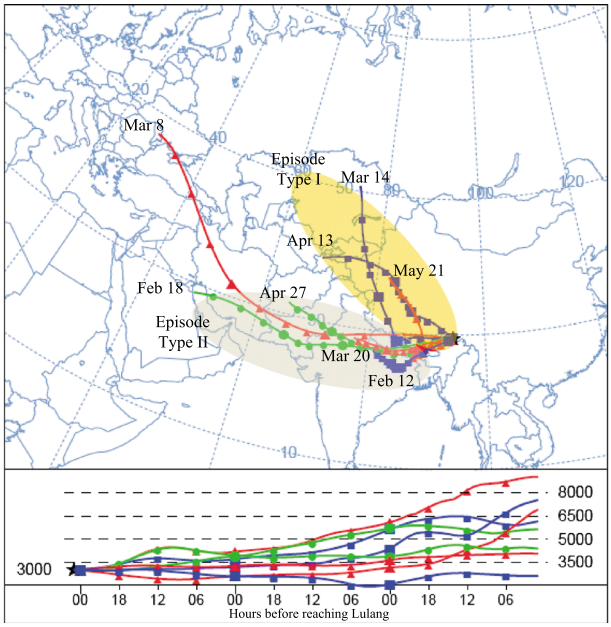

Figure 3. Three day air backward-in-time air mass trajectory analysis for high-aerosol loading episodes at Lulang.

et al., 2002]. Satellite aerosol products considered in this study consist of both level-2.0 aerosol optical depth (AOD) from the Moderate Resolution Imaging Spectrometer (MODIS) which is deployed on the Terra satellite [*Remer et al*., 2005] and the level-2.0G UV aerosol index (AI) derived from the Ozone Monitoring Instrument (OMI) carried by the Aura spacecraft [*Torres et al*., 2007]. MODIS AOD has been shown to be suitable for the detection of aerosol pollution [*Chu et al*., 2003; *Li et al*., 2007], while the OMI AI has been used for long-term remote sensing of UV absorbing aerosols, such as desert dust [*Moulin and Chiapello*, 2004; *Huang et al*., 2007]. Accordingly, we used both MODIS AOD and OMI AI for the case studies described in section 3.4.

2.4. Air Mass Back Trajectory Analysis

[17] Air mass back trajectory analysis is another useful tool for identifying the probable sources and transport pathways for air pollutants. In this study, 72 h air mass back trajectories starting 3000 m above ground level at 0:00 UTC were calculated using the NOAA HYSPLIT4 trajectory model. The trajectories were used to study the origins of the aerosol pollution, and to this end, the high-aerosol loading episodes were classified according to the direction of air mass transport.

2.5. Source Apportionment Method

[18] Receptor modeling by positive matrix factorization (PMF 3.0, developed by the U.S. Environmental Protection Agency) was used to apportion the measured ambient aerosol concentrations among potential sources. PMF can use the information contained in aerosol concentration and composition data to identify presumptive sources. This approach has been widely used for receptor modeling, and it is typically applied when the source profiles are unknown [*Chen et al*., 2007, 2010]. Here PMF was applied as a way of evaluating the origins of the aerosols over the southeastern TP.

3. Results and Discussion

3.1. Variations of Aerosol Mass Concentrations

[19] The arithmetic mean annual aerosol mass concentration was $23.5 \pm 20.3\ \mu g\ m^{-3}$, and it ranged from 8.2 to $139.2\ \mu g\ m^{-3}$. Figure 2 shows the seasonal variations of TSP loadings and major chemical species levels at the Lulang site. The TSP mass exhibits a well-defined seasonal cycle, with the highest mass concentration ($43.7 \pm 37.2\ \mu g\ m^{-3}$) observed during the premonsoon and the lowest value during the monsoon ($14.8 \pm 6.6\ \mu g\ m^{-3}$). The aerosol levels in the premonsoon period were larger by about a factor of 3 compared with mean level during the monsoon; however, the standard deviation of aerosol mass during the premonsoon was much larger than during the monsoon period. This seasonal variation is similar to the aerosol mass and black carbon concentration variations found at the Nepal Climate Observatory at Pyramid (NCO-P) site in the southern Himalayas [*Marinoni et al*., 2010].

[20] High concentrations of aerosol mass and large variability at high elevations, particularly prior to the onset of the monsoon, have been attributed to long-range pollution transport [*Shrestha et al*., 2000]. As shown in Figure 2, major peaks in the TSP mass concentrations always coincided with high loadings of OC, EC, major ions, and Fe. This implies that the same physical processes, including those during both production and transport, caused these species' concentrations to covary. The aerosol mass seasonality we observed at Lulang is similar to the variations observed at other sites in Nepal and India; that is, lower loadings during the monsoon season and higher concentrations in the winter and premonsoon periods [*Ganguly et al*., 2006; *Marinoni et al*., 2010; *Mouli et al*., 2006]. Wet scavenging is one likely cause for the lower aerosol concentrations during the monsoon while in winter, higher aerosol concentrations correspond with diminished precipitation in air brought by strong westerly flow.

[21] Eight high-aerosol loading events, operationally defined by aerosol mass loadings $> 35\ \mu g\ m^{-3}$, were observed during the year of measurements. Two types of high-aerosol episodes were identified on the basis of differences in transport pathways as depicted by back trajectory analysis (Figure 3). Type I episodes (marked in yellow in Figures 2 and 3) were classified as a dust events owing to the abundance of Fe. Three type I events occurred from the premonsoon to monsoon season; these were on 11 to 14 March, 10 to 13 April, and 18 to 21 May. The corresponding aerosol mass loadings for these three events were $139.2\ \mu g\ m^{-3}$, $40.0\ \mu g\ m^{-3}$, and $37.3\ \mu g\ m^{-3}$, giving an arithmetic mean of $72.2\ \mu g\ m^{-3}$, which is over 3 times the yearly mean value.

[22] Type II episodes (marked in gray as shown in Figures 2 and 3) were defined as pollution events because they were characterized by high concentrations of OC, EC, and three major ions (K^+, SO_4^{2-} and NO_3^-). Five type II events occurred over a total of 15 days; one event in winter (9 to 12 February) and four events during the premonsoon period (15 to 18 February, 5 to 8 March, 17 to 20 March, and 23 to 27 April). The mean aerosol mass for type II episodes was $53.8\ \mu g\ m^{-3}$, which is over 2 times the annual value. Chemical profiles for type II episodes were characterized by high K^+/K ratios, indicating important contributions from

Table 2. Arithmetic Averages ± Standard Deviations (μg m^{-3}) for Mass and Chemical Components During Four Seasons

	Premonsoon	Monsoon	Postmonsoon	Winter	Annual	Type I Episode	Type II Episode
N[a]	12	27	6	16	61	3	5
Mass	43.71 ± 37.24	14.78 ± 6.61	18.29 ± 4.84	24.41 ± 6.69	23.49 ± 20.25	72.16 ± 58.03	53.84 ± 23.28
OC	5.15 ± 3.89	4.27 ± 1.23	4.30 ± 1.61	3.65 ± 1.07	4.28 ± 2.05	5.41 ± 0.81	7.93 ± 4.87
EC	0.84 ± 0.55	0.31 ± 0.17	0.67 ± 0.25	0.58 ± 0.16	0.52 ± 0.35	0.61 ± 0.09	1.30 ± 0.57
OC/EC	6.29 ± 1.69	17.67 ± 11.05	6.72 ± 1.86	6.45 ± 1.68	11.41 ± 9.28	9.00 ± 1.58	5.96 ± 1.40
Na^+	0.36 ± 0.19	0.41 ± 0.63	0.20 ± 0.05	0.22 ± 0.12	0.33 ± 0.44	0.38 ± 0.19	0.47 ± 0.20
K^+	0.18 ± 0.29	0.04 ± 0.03	0.03 ± 0.004	0.04 ± 0.02	0.06 ± 0.14	0.04 ± 0.02	0.38 ± 0.39
Mg^{2+}	0.10 ± 0.07	0.08 ± 0.13	0.05 ± 0.01	0.04 ± 0.01	0.07 ± 0.09	0.16 ± 0.08	0.10 ± 0.06
Ca^{2+}	0.56 ± 0.42	0.31 ± 0.13	0.34 ± 0.09	0.27 ± 0.08	0.35 ± 0.23	0.94 ± 0.62	0.55 ± 0.31
Cl^-	0.08 ± 0.11	0.16 ± 0.49	0.06 ± 0.04	0.05 ± 0.05	0.10 ± 0.33	0.22 ± 0.14	0.05 ± 0.06
NO_3^-	0.45 ± 0.60	0.15 ± 0.07	0.17 ± 0.06	0.13 ± 0.06	0.21 ± 0.30	0.33 ± 0.11	0.77 ± 0.86
SO_4^{2-}	2.07 ± 1.82	0.79 ± 0.99	0.75 ± 0.33	0.92 ± 0.55	1.07 ± 1.17	1.59 ± 0.45	3.41 ± 2.18
K	0.90 ± 0.88	0.17 ± 0.19	0.20 ± 0.12	0.38 ± 0.14	0.38 ± 0.50	1.51 ± 1.37	1.11 ± 0.63
Fe	0.88 ± 0.97	0.22 ± 0.22	0.23 ± 0.13	0.50 ± 0.19	0.45 ± 0.55	1.85 ± 1.58	0.99 ± 0.37

[a]Number of samples.

biomass burning upwind. *Xia et al.* [2011] monitored a pollution episode at the Namco site in the central TP from 14 to 19 March 2009, and their results, consistent with ours, indicated that during that time, air pollution was transported to the TP from upwind sources.

[23] The high concentrations of carbonaceous species and major ions during type II episodes can be linked to air flow driven by the SW monsoon; the transport pathways often pass over densely populated areas of the Indo-Gangetic Plain. This region is characterized by heavy anthropogenic emissions, and during the premonsoon season, it is usually dry there [*Marinoni et al.*, 2010]. In contrast, for type I episodes, the back trajectories show a simple flow pattern in which air masses, mainly from western China, bring crustal matter from desert dust source regions to Lulang.

3.2. Chemical Composition

3.2.1. Carbonaceous Aerosol

[24] The abundances of TSP, OC, EC, water-soluble ionic species (WSIS), and OC/EC ratios in the aerosol samples are presented in Table 2 where they are grouped according the type of high-aerosol episode. The overall average concentrations of OC and EC were 4.28 ± 2.05 μg m^{-3} and 0.52 ± 0.35 μg m^{-3}, respectively. Both OC and EC showed distinct seasonal variations with remarkably higher concentrations in late winter into the early premonsoon compared with the other seasons (Figure 2). The EC seasonal trends are in good agreement with the record of EC in ice cores taken from Tibetan glaciers where peaks occur during November to March [*Xu et al.*, 2009]. For OC, the concentrations decreased in the following order: premonsoon (5.15 μg m^{-3}) > monsoon (4.27 μg m^{-3}), and postmonsoon (4.30 μg m^{-3}) > winter (3.65 μg m^{-3}), while EC followed a decreasing order of premonsoon (0.84 μg m^{-3}) > postmonsoon (0.67 μg m^{-3}) > winter (0.58 μg m^{-3}) > monsoon (0.31 μg m^{-3}). The most abundant precipitation occurred during the monsoon (Table 1), and the removal of aerosol particles from suspension by precipitation scavenging was the most likely reason for the lower EC concentrations at that time of year.

[25] The ratios of OC to EC ranged from 1.7 to 8.6, 7.8 to 58.4, 1.9 to 8.4, and 1.7 to 9.6 in premonsoon, monsoon, postmonsoon and winter, respectively; and the corresponding averages were 6.3, 17.7, 6.7, and 6.5. These seasonally averaged OC/EC ratios are comparable with those reported for other high-altitude sites such as Mt. Abu (range: 4.8 to 27.2) and Manora Peak (range: 3.0 to 11.5) [*Ram et al.*, 2008]. Comparisons with other sites on the TP show that the OC concentrations at Lulang (Table 3) were larger than those at the Namco site in the central TP [*Cong et al.*, 2007; *Ming et al.*, 2010]. EC was higher than the value measured at Waliguan in northeast TP [*Wen et al.*, 2001] or Muztagh Ata Mountain, in the western TP [*Cao et al.*, 2009]. These comparisons suggest that Lulang site is more strongly influenced by pollution sources upwind than some other parts of the TP.

[26] The data for the high-aerosol episodes were excluded to characterize the chemical composition of the aerosol on more normal days. OC was found to be more abundant during the monsoon and postmonsoon than in the other two seasons. These trends can be explained by the emission of plant spores and pollen as well as the formation of greater quantities of secondary organic carbon (SOC) in the periods with the higher OC loadings. The average OC (3.88 ± 1.21 μg m^{-3}) and EC (0.44 ± 0.22 μg m^{-3}) concentrations on normal days were ~9 to 14% lower than the annual mean values, and neither OC nor EC showed significant differences on normal days in the four periods (the average OC in four seasons were 2.89, 4.21, 4.30, and 3.52 μg m^{-3}, while EC were 0.50, 0.31,

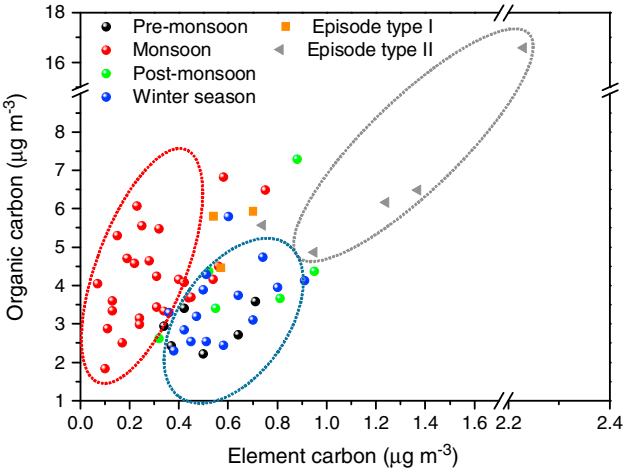

Figure 4. Relationship between the concentrations of organic carbon (OC) and elemental carbon (EC) in four seasons.

Table 3. Comparison of Major Chemical Components From This Study With Measurements at Other Background Sites

Site	Altitude (m asl[a])	Type	Season	Mass	OC	EC(BC)	SO_4^{2-}	NO_3^-	NH_4^+	K^+	Ca^{2+}	Fe	Study
Ahmedabad, India	Unknown	TSP	Annual	139.4	12.8	2.1	4.35	1.43	[b]			4.5	*Rastogi and Sarin* [2009]
Mumbai, India	Unknown	PM_{10}	Mid-Feb to End Mar	128	25.3	12.6	5.5	6.0		8.9	6.2	2.32	*Venkataraman et al.* [2002]
Manora Peak, India	1950	TSP	Winter	27.1	4.9	0.89	2.56	0.5	0.52	0.23	0.75		*Rengarajan et al.* [2007]
Mt. Abu, India	1680	TSP	Wet (May–August)				2.71	0.43	[c]/	0.13	2.39		*Rastogi and Sarin* [2005]
			Dry (Jan–Apr, Sep–Dec)				3.08	0.74	0.37	0.2	1.67		
NCO-P, Nepal	5079	PM_{10}	Premonsoon		2.4	0.5	1.48	0.66	0.52	0.12	0.34		*Decesari et al.* [2010]
			Monsoon		0.9	0.1	0.50	0.37	0.00	0.05	0.00		
			Postmonsoon		1.4	0.1	0.50	0.00	0.02	0.02	0.01		
			Winter Season		1.2	0.1	0.22	0.08	0.02	0.02	0.10		
ABC-Pyramid Observatory, Nepal	5079	PM_{10}	Premonsoon	5.4		0.468[d]							*Bonasoni et al.* [2008]
Nam Co, Central Tibet	4730	TSP	Jul–Oct		0.476	0.008						0.094	*Ming et al.* [2010]/*Cong et al.* [2007]
			Nov–Feb		1.572	1.77							
Waliguan, Northeast Tibet	3814		Annual			0.135						1.72–3.91	*Wen et al.* [2001]
Muztagh Ata Mountain, Western Tibet	4500	TSP	Spring		0.36	0.038							*Cao et al.* [2010]
			Summer		0.77	0.071							
			Autumn		0.4	0.062							
			Winter		0.37	0.052							
Lulang, Southeast Tibet	3360	TSP	Premonsoon	43.71	5.15	0.84	2.07	0.45	/	0.18	0.56	0.88	This Study
			Monsoon	14.78	4.27	0.31	0.79	0.15	/	0.04	0.31	0.22	
			Postmonsoon	18.29	4.30	0.67	0.75	0.17	/	0.03	0.34	0.23	
			Winter season	24.41	3.65	0.58	0.92	0.13	/	0.04	0.27	0.50	

[a]asl stands for above sea level.
[b]Blanks indicate no data.
[c]/ indicates below detection limit.
[d]TSP.

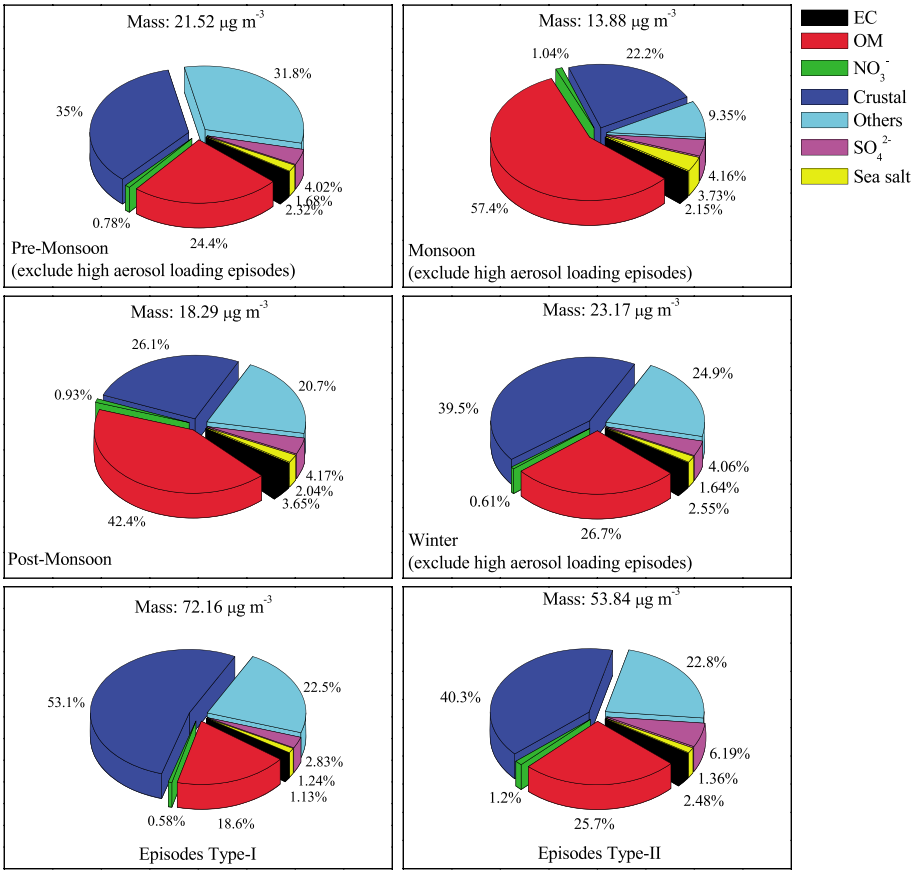

Figure 5. Seasonal and episodic variations of mass concentrations and fractions of organic matter, elemental carbon, nitrate, sulfate, sea salt, and crustal material normalized to aerosol mass concentration.

0.67 and 0.57 μg m^{-3}, respectively). During type II episodes, the average OC and EC concentrations reached 7.93 (4.86 to 16.58) and 1.30 (0.74 to 2.23) μg m^{-3}, these were much higher than those during type I episodes or on normal days. The higher OC and EC levels in the type II samples imply that compared with the others, combustion sources were stronger contributors during the type II events.

[27] The OC and EC concentrations were generally well correlated, with a least squares linear regression for the full data set yielding the following equation: $OC = 4.1 \times EC + 2.1$ (with a correlation coefficient $r = 0.70$ and probability for chance occurrence $p < 0.0001$, $n = 61$). Relationships between the concentrations of OC and EC in the monsoon and other periods are shown in Figure 4 to illustrate the seasonal differences in aerosol characteristics. However, the correlations for the four separate seasons are relatively lower ($r = 0.3$ to 0.6) than the entire data set; this suggests the existence of multiple sources of OC and EC that were not always linked.

3.2.2. Water-Soluble Ionic Species (WSIS)

[28] The sums of the concentrations of the eight ions analyzed were 3.81, 1.92, 1.60, and 1.67 μg m^{-3} in the premonsoon, monsoon, postmonsoon, and winter samples, respectively, and these sums amounted to 16.24%, 8.17%, 6.81%, and 7.10% of the total TSP mass. The dominant compounds were SO_4^{2-}, Ca^{2+}, and NO_3^-, whose combined concentrations accounted for more than 75% of the total water-soluble ion mass. Ion mass balance calculations were used to evaluate the acid-base balance of aerosol and to determine whether significant quantities of undetected ions were present in the samples [*Jain et al.*, 2000]. A strong correlation ($r = 0.87$) between cation and anion equivalents for all samples implies that the ions measured in our study were in fact the most abundant ions on the filters. The ratio of anion to cation equivalents was ~0.86, which was higher than the ratios determined at Zhuzhang and Lhasa, Tibet [*Qu et al.*, 2008; *Tang et al.*, 2005], and this suggests that the Lulang TSP is more alkaline than the aerosol from the other two sites.

[29] Interestingly, most of the NH_4^+ values were below the detection limit (data not shown in Table 1)—the exceptions were samples collected during three heavy pollution events (15 to 18 February, 5 to 8, and 17 to 20 March). Indeed, the aerosol during type I episodes was depleted in NH_4^+ compared with the samples collected during type II episodes. Prior studies have similarly shown depletions in NH_4^+ during dust storm events compared with pollution events [*Shen et al.*, 2009]. The pattern in NH_4^+ concentrations at Lulang is similar to what was observed in previous studies at the NCO-P site on the southern Himalayas. There the ammonium levels also were below the detection limit except during the premonsoon [*Decesari et al.*, 2010]. The low concentrations of ammonium at these high-latitude sites highlight the somewhat usual ion profiles of particular matter (PM) from the TP; one implication of the low NH_4^+ loadings is that other cations, such as Ca^{2+} and Mg^{2+}, should play relatively more important roles in ion balance.

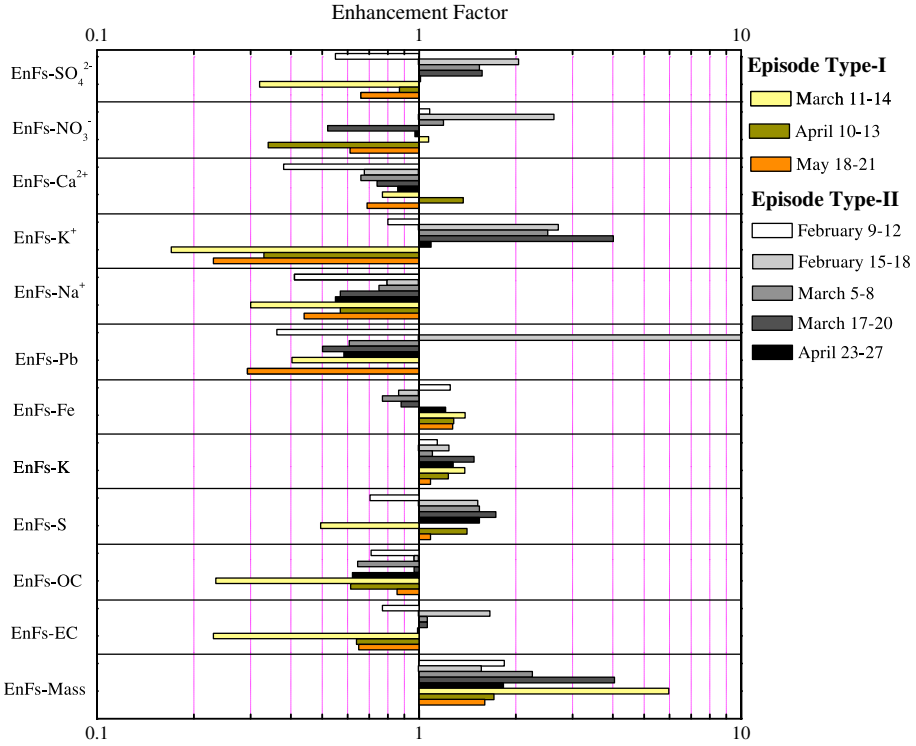

Figure 6. Enhancement factors for selected species in total suspended particles at Lulang during eight high-aerosol loading events. The enhancement factor for species *i* (EnF_i) is the ratio of that species' TSP mass fraction on the designated date to the ratio of its annual average concentration to the annual average of TSP (i.e., $EF_{ik} = F_{ik} / \left(\sum_{n=1}^{K} F_{ik} TSP_n / \sum_{n=1}^{K} TSP_n\right)$, where EnF_{ik} = enhancement factor for species *i* on sample *k*, F_{ik} = ratio of species *i* concentration to TSP concentration on sample *k*, *K* total number of samples, and TSP_n = TSP concentration on sample n).

[30] In the data sets with the high-aerosol events excluded, none of the ions showed significant variations except for Na^+ and Cl^-; this implies that there were no substantial changes in the pollution sources under clean background conditions. The rank order for the most abundant to least abundant ionic species followed the sequence $SO_4^{2-} > Na^+ > Ca^{2+} > NO_3^- > Cl^-$; $> Mg^{2+} > K^+ > NH_4^+$. In the monsoon season, when winds are predominantly from the Arabian Sea, the concentrations of Na^+ and Cl^- were relatively high (average: 0.42 and 0.16 μg m^{-3}, respectively), in fact, twice the loadings in the other periods. This pattern is similar to the seasonality in sea salt observed at Mt Abu, India [*Rastogi and Sarin*, 2005].

[31] Previous studies have shown that biomass burning is a major source of aerosol particles in Southern Asia [*Chan et al.*, 2003; *Duncan et al.*, 2003]. The concentrations of K^+, a tracer of biomass burning [*Andreae*, 1983; *Shen et al.*, 2009], in aerosol samples during the type II episodes (0.38 μg m^{-3}) were much higher than those in the premonsoon (0.04 μg m^{-3}), monsoon (0.04 μg m^{-3}), postmonsoon(0.03 μg m^{-3}), winter seasons (0.03 μg m^{-3}), or type I episodes (0.04 μg m^{-3}). This can be explained by strong emissions from biomass burning sources upwind of the measurement site during the type II episodes. The concentrations of SO_4^{2-} and NO_3^- during these episodes also were enhanced by factors of 4 to 5 over those on normal days. The elevated loadings of K^+, along with SO_4^{2-}, NO_3^-, OC, and EC in the type II samples, suggest that emissions from a combination of biomass burning and fossil fuel combustion sources were brought to Lulang during those episodes, mostly likely as a result of long-range transport.

3.3. Material Balance

[32] The relative contributions of major chemical species to the aerosol mass for different seasons (excluding the pollution events) as well as during two type episodes are shown in Figure 5. Organic matter (OM) concentrations were calculated as 1.8 times the OC content as suggested by *Turpin and Lim* [2001]. Sea salt was estimated from $Cl^- + (1.4486 \times Na^+)$ where 1.4486 is the ratio of the sum concentration of all elements except Cl^- in sea water to the concentration of Na^+ [*Li et al.*, 2010]. Crustal matter (geological material) was calculated by Fe/4% [*Zhang et al.*, 2003].

[33] The sums of the measured and estimated components accounted for 68, 91, 79, and 79% of the aerosol mass in the premonsoon, monsoon, postmonsoon, and winter samples, respectively. During the premonsoon, crustal matter was the most abundant species, followed by OM, sulfate, EC, sea salt, and nitrate. In contrast, during the monsoon and postmonsoon, OM dominated, accounting for 57% and 42% of the mass, respectively, and crustal matter decreased when compared with the premonsoon period. Sea salt accounted for only 1.7% of the aerosol mass in the premonsoon and winter season, but the percentage did increase by a factor of ~2.2 during the monsoon. For the winter samples, the contributions in order of importance were geological material > OM > sulfate > elemental carbon > sea salt > nitrate. Approximately 9 to 32% of the measured mass was not quantified by the chemical analysis, and this can be ascribed to residual water and other unmeasured species, underestimations of the weighting factors for OM, sea salt, and geological material. Possible errors in

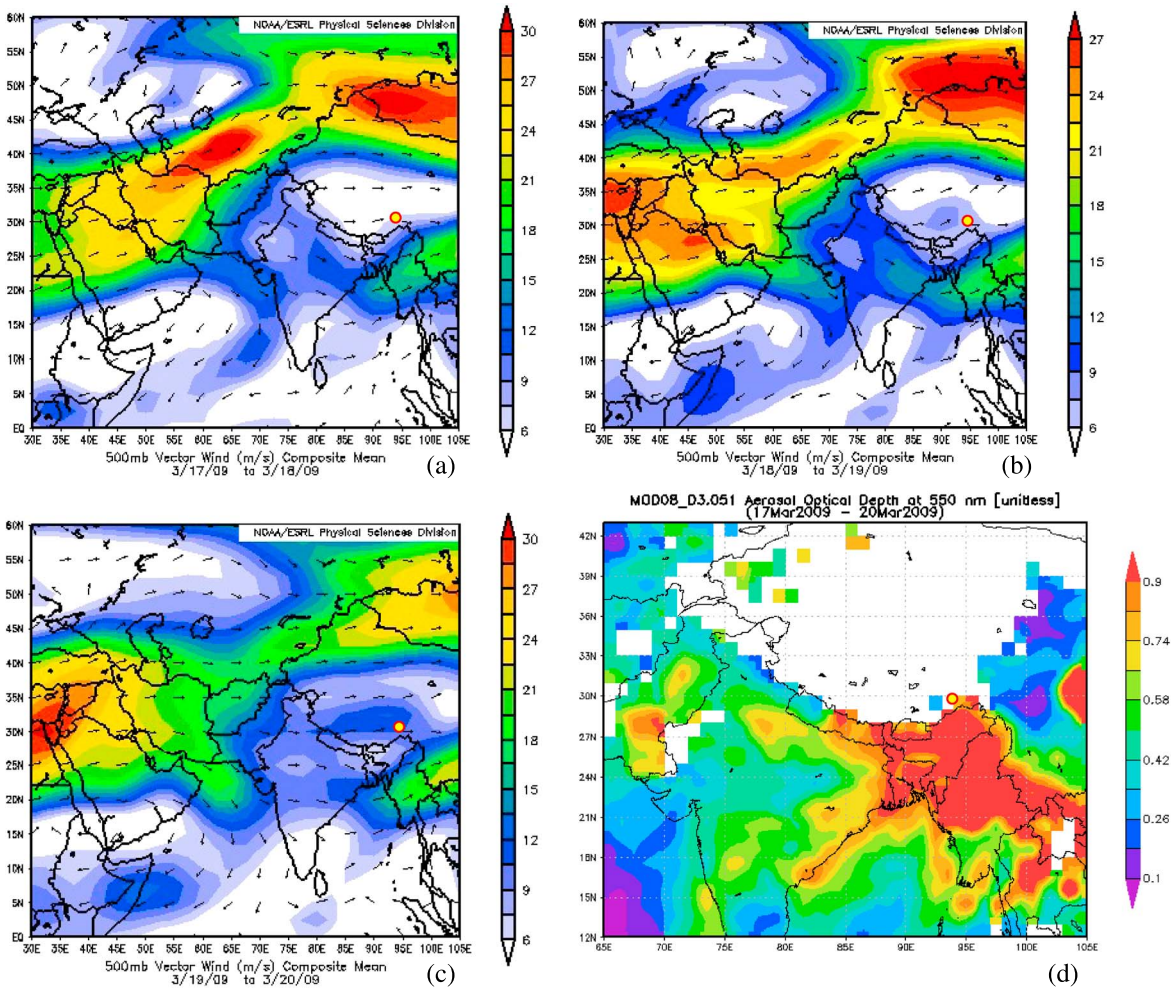

Figure 7. NCEP/NCAR wind trajectory analysis at 500 hPa and satellite (MODIS) integrated aerosol optical depth (AOD) for typical high-aerosol episode days: (a, b, and c) NCEP/NCAR wind trajectories for 17 to 20 March and (d) average AOD for 17 to 20 March. (The yellow circle: sampling site).

the gravimetric analyses, which would mainly be due to uncertainties in the equilibration of the filters [*Kajino et al*., 2006], also must be acknowledged.

[34] During type I events, crustal matter was the most abundant aerosol constituent, contributing 53% to the mass, and it was followed by OM (19%). These results can be compared with data for the dust storm observed at Zhenbeitai; in that study, mineral dust contributed 51% to the $PM_{2.5}$ mass, followed by carbonaceous matter (12%) [*Xu et al*., 2004]. For type II episodes, the percentage of the aerosol mass contributed by crustal matter decreased to 40%, while the percentages of sulfate, nitrate, and EC increased; these are relatively similar to their contributions in the premonsoon and winter. The high crustal material loadings and high sulfate, nitrate, and EC, in terms of both concentration and percentage, show that both geological and anthropogenic sources provided significant quantities of the aerosol that was transported to the southeastern TP in type II episodes.

3.4. Species Enhancements During High-Aerosol Episodes

[35] Enhancement factors (EnF, plural EnFs) are defined here as the ratio of the mass fraction for a species during the eight high-aerosol episodes normalized to the annual average mass fraction (see text for description of enhancement factors in the caption of Figure 6) [*Watson et al*., 2002]. Here we calculate the EnFs to further investigate the chemical composition of PM during the high-aerosol loading events (Figure 6).

[36] For all events, the EnFs of OC and Na^+ were less than unity, showing that these species did not contribute significantly to the high-aerosol loads. In addition, as Figure 6 shows, the EnFs of most combustion- and industry-related species (K^+, SO_4^{2-}, EC) showed mass fractions less than the annual average (EnFs < 1) for the 21 May, 13 April, and 14 March 2009 episodes, and the moderate enhancement of crustal K for these days is consistent with regional transport from the northwest. For the type II episodes (typical haze events), the EnFs for K^+, SO_4^{2-} were relatively high, while the EnFs for NO_3^-, S, and K were lower. Compared with type I episodes, the EnFs for the type II events seem to be more variable, and it is worth noting that the EnFs for each of these pollution events were different from one other.

[37] During one severe episode (15 to 18 February), several species associated with combustion products

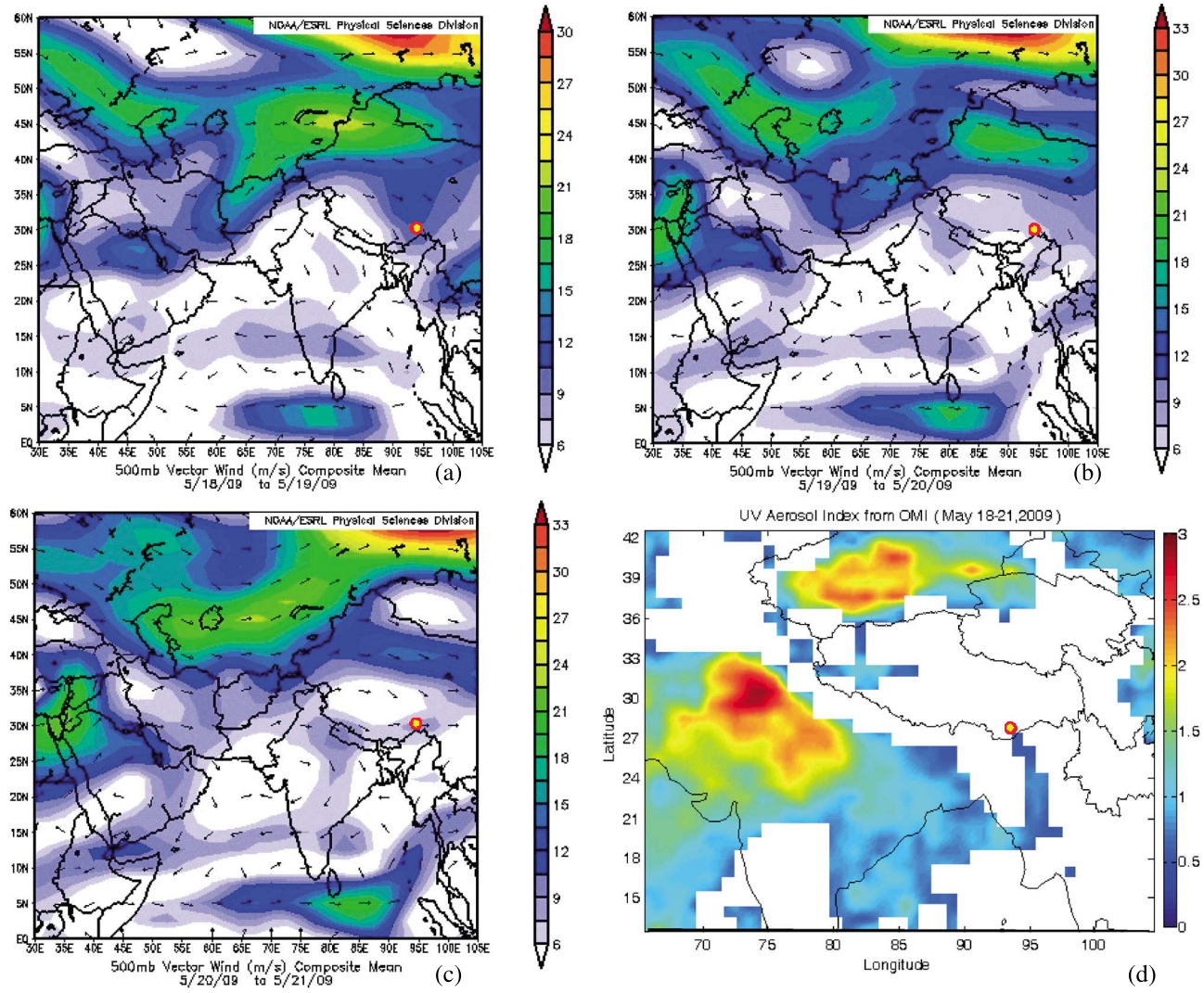

Figure 8. NCEP/NCAR wind trajectory integrated UV-AI (OMI) for typical episode days: (a, b, and c) NCEP/NCAR wind trajectories for 18 to 21 May and (d) UV-AI from OMI for 17 to 20 March.

(NO_3^-, SO_4^{2-}, Pb, and K^+) showed significant enhancements (EnFs: 2 to 10), and this is an indication that the high-aerosol load during this episode was due, at least in part, to emissions produced from fossil fuel combustion. In contrast, the EnFs for crustal matter (Fe) and Ca^{2+} were less than unity during the event, indicating a relatively small contribution from dust. This haze episode evidently was influenced by a combination of strong anthropogenic emissions on Indian subcontinent coupled with dry meteorological conditions during regional transport; this conclusion also is supported by back trajectory analysis (as shown in Figure 3).

[38] During another episode (17 to 20 March), K^+ and K were the most strongly enhanced components of all measured species (EnFs of 4.0 and 1.5, respectively), and the EnFs for NO_3^-, EC, SO_4^{2-}, and S also were relatively high. This can be explained by the transport of polluted boundary layer air enriched with products from biomass burning and fossil fuel combustion. The EnF analysis indicated that several kinds of pollutants were enhanced several fold as a result of transport from upwind regions, and this is important because anthropogenic substances can exert several types of influences on the environment and climate of the TP; these effects include alterations of the radiative balance as well as melting the glaciers on the TP.

3.5. Further Evidence for Long-Range Aerosol Transport

[39] The seasonally averaged levels of TSP, EC, OC, and ions are compared with other measurements from the TP, Nepal, and the Indian Peninsula in Table 3. The concentrations of OC, EC, and ions are comparable with those at two high-altitude sites—the Atmospheric Brown Cloud-Pyramid Observatory [*Bonasoni et al.*, 2008] and NCO-P [*Decesari et al.*, 2010]—but they are much lower than those on the Indian subcontinent [*Rastogi and Sarin*, 2005, 2009; *Rengarajan et al.*, 2007; *Venkataraman et al.*, 2002], especially urban sites (Ahmedabad and Mumbai). Such comparisons along with the air flow analyses (see below) suggest that the high-aerosol emissions over the Indian Peninsula were major influences on the TP air.

[40] To further investigate the transport of anthropogenic aerosol to the southeastern TP, we analyzed National

Figure 9. Source apportionments by positive matrix factorization (PMF) receptor model. (a) Source profiles for total suspended particles from PMF, (b) factor contributions from PMF in relation to sampling time, and (c) factor loading for TSP mass (yellow arrow: episode type I; gray arrow: episode type II).

Centers for Environmental Protection/National Center for Atmospheric Research (NCEP/NCAR) winds at 500 hPa, the corresponding MODIS AOD at 550 nm, and the ultraviolet aerosol index values (UV-AI) from the Ozone Monitoring Instrument for two typical episodes (Figures 7 and 8). These two figures are comprehensive maps of the spatial distributions of AOD/AI over the study region. Daily NCEP/NCAR reanalysis wind trajectories were used to determine the daily trends in the wind directions during the episodes.

[41] As shown in Figure 7, the 17 to 20 March high-aerosol episode had the highest concentrations of SO_4^{2-}, NO_3^-, K^+, OC, and EC (Figure 2) of all the events. For this case, the wind direction in the vicinity of the measurement site was from the west or southwest, with a mean speed of 10 m s^{-1}. The air mass passed over the Thar Desert, located in northwestern India, and this was likely responsible for the high-dust load during this period. Results from MODIS showed that Lulang was shrouded in high-aerosol loads at this time, with the AOD value exceeding 0.9 (Figure 7d). The remarkably high AOD area stretched along the southern slope of the Himalayas (including southeastern India and areas east of Nepal and northeast of Myanmar) during this episode, and the information on wind fields and AOD in Figure 7 clearly indicates a likely pathway for pollutants as they were transported to Lulang. Another recent study similarly showed that high BC concentrations at Lulang were associated with the transport from the southwest [*Cao et al*., 2010].

[42] Figure 8 shows that the high mass and high Fe (dust) concentrations observed from 18 to 21 May were associated with northwesterly winds with speeds of <10 m s^{-1}. The OMI AI in the northern TP (regions adjacent to the Taklimakan Desert and Qaidam Desert) and in northwestern India (parts of the Thar-Cholistan Desert) were high, that is, >2 (Figure 8d). The NCEP/NCAR wind trajectories showed that winds from the northwest prevailed during the period, and the patterns in OMI AI suggest that the winds carried large quantities of geological material to the site. In contrast, the concentrations of combustion products (SO_4^{2-}, NO_3^-, K^+, and EC) during this period were relatively low. Other studies conducted at this sampling site have shown that transport from northwest was associated with low BC levels but high-dust loadings [*Cao et al*., 2010; *Xia et al*., 2008].

3.6. Source Apportionment With the Use of a PMF Model

[43] All of the aerosol data, that is, the concentrations of OC, EC, S, K, Ca, Ti, Fe, Na^+, K^+, Mg^{2+}, Ca^{2+}, Cl^-, NO_3^-, and SO_4^{2-}, were included in PMF analyses, which followed the procedures described in Reff *et al*. (2007) and *Green et al*. (2012). The frequency distribution of scaled residuals was taken into account in the model; most of these were between -2 and $+2$, and this attests to a good agreement between the PMF model results and the input data. The profiles for each factor and the factor loadings are shown in Figure 9.

[44] Factor 1 was dominated by OC, EC, K, K^+, Ti, and Fe (Figure 9a), and it is best interpreted as a mixture of dust and combustion aerosol. It is noteworthy that the Factor 1 contribution to TSP mass was high in premonsoon season (Figure 9b), especially from 15 to 18 February, 5 to 8 March, 17 to 20 March, and 23 to 27 April. All of these intervals were characterized as type II high-aerosol events. This result is also supported by air mass back trajectories and MODIS AODs, which provide evidence for the long-range transport of mixed aerosols from the Indo-Gangetic Plain along the valley of the Yarlung Tsangpo River to the southeastern TP. Nearly one third of the TSP mass was accounted for by this factor (Figure 9c).

[45] The second PMF factor had high loadings for Na^+, K^+, Mg^{2+}, Ca^{2+}, Cl^-, and OC, and this factor is most readily explained as a combination of SOC and sea salt. The Factor

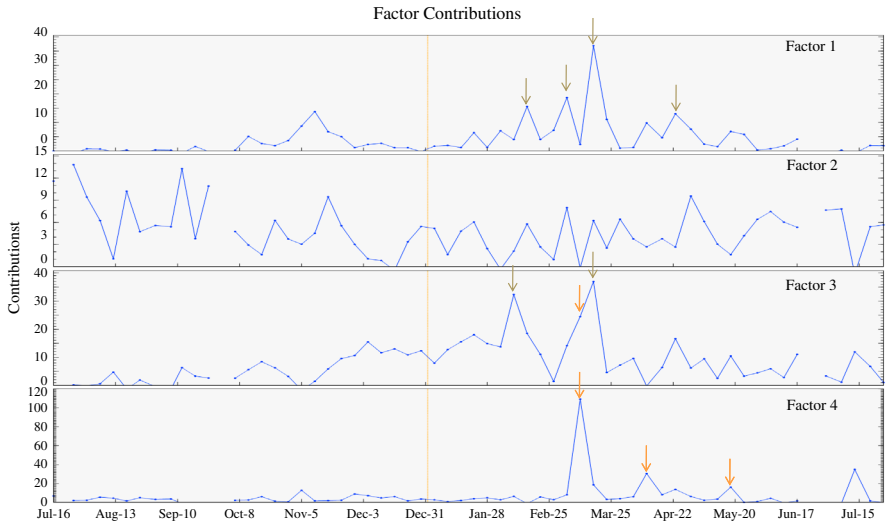

(b)

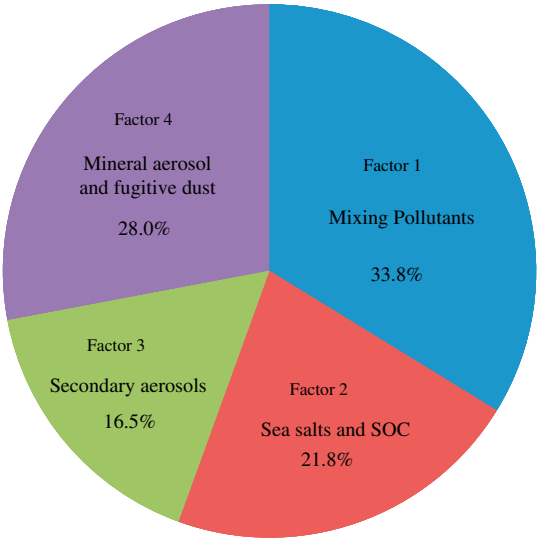

(c)

Figure 9. (continued)

2 contribution was higher in summer, and this factor accounted for 22% of annual TSP mass.

[46] The NO_3^-, SO_4^{2-}, and sulfur concentrations in the profiles of the third factor were very high, and this can be attributed to the formation of secondary aerosols. The highest contribution from Factor 3 occurred from 9 to 12 February and 17 to 20 March (marked by gray arrows in Figure 9b). The strong loadings of Factor 3, combined with air mass trajectories for these dates, indicated that aged air that had passed over the Indo-Gangetic Plain carried high loadings of secondary aerosols to Lulang. We note that the sample collected from 11 to 14 March (yellow arrow) had a large contribution from both Factor 3 (secondary aerosol) and Factor 4 (dust storms). This can be explained by the back trajectory analysis (Figure 3) which also is substantiated by the wind directions determined from the NCEP/NCAR reanalysis (Figure 10). That is, from 13 to 14 March, the wind direction at Lulang changed from northwest to southwest, and therefore, one can see how this flow could bring a mixture of crustal matter from the northwest and secondary pollutants from the southwest to our sampling site. The back trajectory for this period (Figure 3) shows how the air flow changed course and passed over the northern edge of India before arriving at the southeastern TP. This factor accounted for 17% of the annual average TSP mass, and high contributions occurred in the winter and premonsoon season.

[47] Factor 4 was enriched in crustal elements (e.g., Ca, Fe, Ti, K, Mg^{2+}, Ca^{2+}, and Cl^-), and this factor clearly represents mineral aerosol and fugitive dust. In the same way as Factor 1, major contributions occurred during 11 to 14 March, 10 to 13 April, and 18 to 21 May (marked by yellow arrows in Figure 9b); these were all characterized as type I episodes. This factor accounted for 28% of TSP mass.

4. Summary and Conclusions

[48] One year of continuous observations of aerosol composition (from July 2008 to July 2009) were conducted at Lulang (3300 m above sea level) on the southeastern TP. The data set provides insights into the chemical composition and the sources of aerosols over a remote, high-altitude site on the TP. Major results were summarized as below.

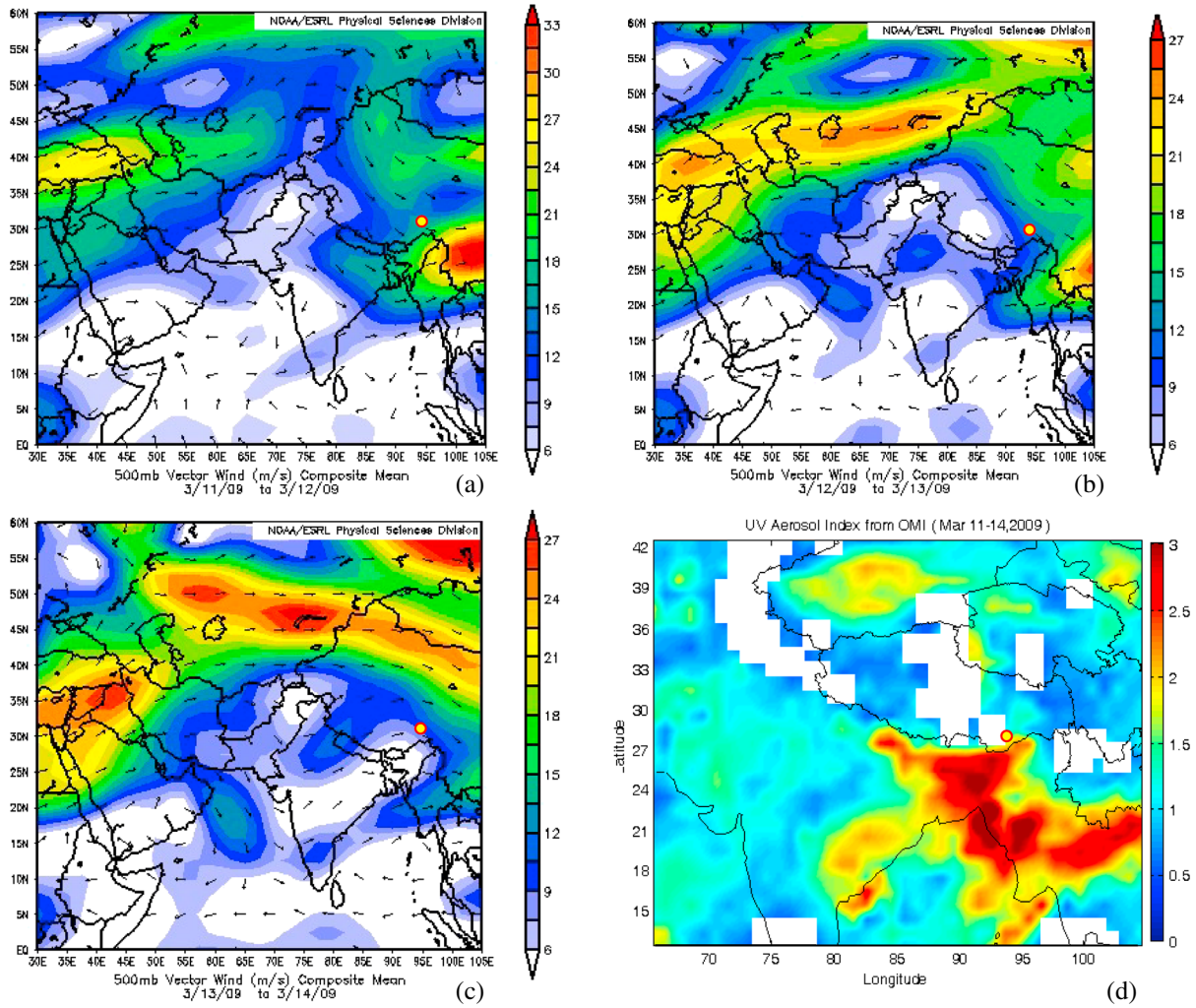

Figure 10. Detailed wind patterns and the corresponding ultraviolet aerosol index (AI) distributions from the Ozone Monitoring Instrument: (a, b, and c) NCEP/NCAR wind trajectories for 11 to 14 March and (d) UV-AI for 11 to 14 March.

[49] 1. During the premonsoon, the highest seasonal values of TSP, OC, EC, K^+, NO_3^-, and SO_4^{2-} were observed, while the lowest concentrations of EC and TSP occurred during the monsoon, and OC was lowest in winter. The clear seasonal variations of these compounds at Lulang can be explained by seasonal differences in atmospheric conditions.

[50] 2. Source apportionment by PMF produced four factors of the TSP mass; there were (1) mixed dust and combustion aerosols, (2) SOC and sea salt, (3) secondary aerosols, and (4) mineral aerosol and fugitive dust. The mixed dust and pollution factor was the largest contributor, accounting for 33.8% of TSP mass, followed by mineral aerosol and fugitive dust (28.0%). The highest contributions for these two factors were coincident with the high-aerosol episodes, and the interpretations were supported by air mass back trajectory and MODIS AOD analyses.

[51] 3. The concentrations of major chemical species increased several fold during pollution episodes compared with normal days. Evidence obtained from back trajectories and NCEP/NCAR reanalysis highlighted the impact of pollution from northern India on the southeastern TP.

[52] Further studies are needed to better understand the sources and transport of anthropogenic particles from South Asia and dust particles from the surrounding deserts; additional studies also are needed to reveal their potential climatic and environmental impacts.

[53] **Acknowledgments.** This study was supported by the National Natural Science Foundation of China (41230641, 40925009) and projects from the "Strategic Priority Research Program" of the Chinese Academy of Science (grant XDA05100401). The authors are grateful to Haiqing Xu and Yongjie Wang for their assistance in the aerosol sampling and analyses. Special thanks should go to Darrel Baumgardner for his kind help with grammar revising.

References

An, Z. S., J. E. Kutzbach, W. L. Prell, and S. C. Porter (2001), Evolution of Asian monsoons and phased uplift of the Himalaya-Tibetan plateau since Late Miocene times, *Nature*, *411*(6833), 62–66.

Andreae, M. O. (1983), Soot carbon and excess fine potassium: Long-range transport of combustion-derived aerosols, *Science*, *220*(4602), 1,148–1,151.

Bonasoni, P., et al. (2008), The ABC-Pyramid Atmospheric Research Observatory in Himalaya for aerosol, ozone and halocarbon measurements, *Sci. Total Environ.*, *391*(2–3), 252–261.

Bonasoni, P., et al. (2010), Atmospheric brown clouds in the Himalayas: First two years of continuous observations at the Nepal Climate Observatory-Pyramid (5079 m), *Atmos. Chem. Phys.*, *10*(15), 7515–7531.

Byson, R. A. (1986), *Airstream Climatology of Asia*, American Meteorological Society, Boston, pp. 604–617.

Cao, J. J., B. Q. Xu, J. Q. He, X. Q. Liu, Y. M. Han, G. H. Wang, and C. S. Zhu (2009), Concentrations, seasonal variations, and transport of carbonaceous aerosols at a remote mountainous region in western China, *Atmos. Environ.*, *43*(29), 4444–4452.

Cao, J. J., S. C. Lee, K. F. Ho, X. Y. Zhang, S. C. Zou, K. Fung, J. C. Chow, and J. G. Watson (2003), Characteristics of carbonaceous aerosol in Pearl River Delta Region, China during 2001 winter period, *Atmos. Environ.*, *37*(11), 1451–1460.

Cao, J. J., X. X. Tie, B. Q. Xu, Z. Z. Zhao, C. S. Zhu, G. H. Li, and S. X. Liu (2010), Measuring and modeling black carbon (BC) contamination in the SE Tibetan Plateau, *J. Atmos. Chem.*, *67*(1), 45–60.

Cao, J. J., Z. X. Shen, J. C. Chow, J. G. Watson, S. C. Lee, X. X. Tie, K. F. Ho, G. H. Wang, and Y. M. Han (2012), Winter and summer PM2.5 chemical compositions in fourteen Chinese cities, *J. Air Waste Manage.*, *62*(10), 1214–1226, doi:10.1080/10962247.2012.701193.

Carrico, C. M., M. H. Bergin, A. B. Shrestha, J. E. Dibb, L. Gomes, and J. M. Harris (2003), The importance of carbon and mineral dust to seasonal aerosol properties in the Nepal Himalaya, *Atmos. Environ.*, *37*(20), 2811–2824.

Chan, C. Y., L. Y. Chan, J. M. Harris, S. J. Oltmans, D. R. Blake, Y. Qin, Y. G. Zheng, and X. D. Zheng (2003), Characteristics of biomass burning emission sources, transport, and chemical speciation in enhanced spring-time tropospheric ozone profile over Hong Kong, *J. Geophys. Res.*, *108*(D1), 4015, doi:10.1029/2001JD001555.

Chen, L.-W. A., J. G. Watson, J. C. Chow, and K. L. Magliano (2007), Quantifying $PM_{2.5}$ source contributions for the San Joaquin Valley with multivariate receptor models, *Environ. Sci. Technol.*, *41*(8), 2818–2826.

Chen, L. -W. A., D. H. Lowenthal, J. G. Watson, D. Koracin, N. Kumar, E. M. Knipping, N. Wheeler, K. Craig, and S. Reid (2010), Toward effective source apportionment using positive matrix factorization: Experiments with simulated $PM_{2.5}$ Data, *J. Air Waste Manage. Assoc.*, *60*, 43–54.

Chow, J. C., J. G. Watson, L. W. A. Chen, M. C. O. Chang, N. F. Robinson, D. Trimble, and S. Kohl (2007), The IMPROVE: A temperature protocol for thermal/optical carbon analysis: Maintaining consistency with a long-term database, *J. Air Waste Manage. Assoc.*, *57*(9), 1014–1023.

Chu, D. A., Y. J. Kaufman, G. Zibordi, J. D. Chern, J. Mao, C. Li, and B. N. Holben (2003), Global monitoring of air pollution over land from the Earth Observing System-Terra Moderate Resolution Imaging Spectroradiometer (MODIS), *J. Geophys. Res.*, *108*(D21), 4661, doi:10.1029/2002JD003179.

Cong, Z. Y., S. C. Kang, X. D. Liu, and G. F. Wang (2007), Elemental composition of aerosol in the Nam Co region, Tibetan Plateau, during summer monsoon season, *Atmos. Environ.*, *41*(6), 1180–1187.

Decesari, S., et al. (2010), Chemical composition of PM_{10} and PM_1 at the high-altitude Himalayan station Nepal Climate Observatory-Pyramid (NCO-P) (5079m a.s.l.), *Atmos. Chem. Phys.*, *10*, 4583–4596.

Duncan, B. N., R. V. Martin, A. C. Staudt, R. Yevich, and J. A. Logan (2003), Interannual and seasonal variability of biomass burning emissions constrained by satellite observations, *J. Geophys. Res.*, *108*(D2), 4100, doi:10.1029/2002JD002378.

Engling, G., Y.-N. Zhang, C.-Y. Chan, X.-F. Sang, M. Lin, K.-F. Ho, Y.-S. Li, and J. J. Lee (2011), Characterization and sources of aerosol particles over the southeastern Tibetan Plateau during the Southeast Asia biomass-burning season, *Tellus B*, *63*(1), 117–128.

Ganguly, D., A. Jayaraman, T. A. Rajesh, and H. Gadhavi (2006), Wintertime aerosol properties during foggy and nonfoggy days over urban center Delhi and their implications for shortwave radiative forcing, *J. Geophys. Res.*, *111*, D15217, doi:10.1029/2005JD007029.

Green, M. C., L.-W. A. Chen, D. W. DuBois, and J. V. Molenar (2012), Fine particulate matter and visibility in the Lake Tahoe Basin: Chemical characterization, trends, and source apportionment, *J. Air Waste Manage. Assoc.*, *62*(8), 953–965.

Hindman, E. E., and B. P. Upadhyay (2002), Air pollution transport in the Himalayas of Nepal and Tibet during the 1995–1996 dry season, *Atmos. Environ.*, *36*(4), 727–739.

Huang, J., P. Minnis, Y. Yi, Q. Tang, X. Wang, Y. Hu, Z. Liu, K. Ayers, C. Trepte and D. Winker (2007), Summer dust aerosols detected from CALIPSO over the Tibetan Plateau, *Geophys. Res. Lett.*, *34*, L18805, doi:10.1029/2007GL029938.

Jain, M., U. C. Kulshrestha, A. K. Sarkar, and D. C. Parashar (2000), Influence of crustal aerosols on wet deposition at urban and rural sites in India, *Atmos. Environ.*, *34*(29–30), 5129–5137.

Kajino, M., W. Winiwarter, and H. Ueda (2006), Modeling retained water content in measured aerosol mass, *Atmos. Environ.*, *40*(27), 5202–5213.

Kaufman, Y. J., D. Tanré, and O. Boucher (2002), A satellite view of aerosols in the climate system, *Nature*, *419*, 215–223, doi:10.1038/nature01091.

King, D. M., Y. J. Kaufman, D. Tanré, and T. Nakajima (1999), Remote sensing of tropospheric aerosols from space: Past, present, and future, *Bull. Am. Meterol. Soc.*, *80*(11), 2,229–2,259, doi:10.1175/1520-0477(1999)080.

Lau, W. K. M., M.-K. Kim, K.-M. Kim, and W.-S. Lee (2010), Enhanced surface warming and accelerated snow melt in the Himalayas and Tibetan Plateau induced by absorbing aerosols, *Environ. Res. Lett.*, *5*(2), doi:10.1088/1748-9326/5/2/025204.

Li, L., W. Wang, J. L. Feng, D. P. Zhang, H. J. Li, Z. P. Gu, B. J. Wang, G. Y. Sheng, and J. M. Fu (2010), Composition, source, mass closure of $PM_{2.5}$ aerosols for four forests in eastern China, *J. Environ. Sci.*, *22*(3), 405–412.

Li, L. J., Y. Wang, Q. Zhang, T. Yu, Y. Zhao, and J. Jin (2007), Spatial distribution of aerosol pollution based on MODIS data over Beijing, China, *J. Environ. Sci.*, *19*(8), 955–960.

Marinoni, A., et al. (2010), Aerosol mass and black carbon concentrations, a two year record at NCO-P (5079 m, Southern Himalayas), *Atmos. Chem. Phys.*, *10*, 8551–8562.

Ming, J., C. D. Xiao, J. Y. Sun, S. C. Kang, and P. Bonasoni (2010), Carbonaceous particles in the atmosphere and precipitation of the Nam Co region, central Tibet, *J. Environ. Sci.*, *22*(11), 1748–1756.

Mouli, P., S. Mohan, and S. Reddy (2006), Chemical composition of atmospheric aerosol (PM_{10}) at a semi-arid urban site: Influence of terrestrial sources, *Environ. Monit. Assess.*, *117*(1), 291–305.

Moulin, C., and I. Chiapello (2004), Evidence of the control of summer atmospheric transport of African dust over the Atlantic by Sahel sources from TOMS satellites (1979–2000), *Geophys. Res. Lett.*, *31*, L02107, doi:10.1029/2003GL018931.

Qu, W. J., X. Y. Zhang, R. Arimoto, D. Wang, Y. Q. Wang, L. W. Yan, and Y. Li (2008), Chemical composition of the background aerosol at two sites in southwestern and northwestern China: Potential influences of regional transport, *Tellus B*, *60*(4), 657–673.

Ram, K., M. M. Sarin, and P. Hegde (2008), Atmospheric abundances of primary and secondary carbonaceous species at two high-altitude sites in India: Sources and temporal variability, *Atmos. Environ.*, *42*(28), 6785–6796.

Ramanathan, V., and P. J. Crutzen (2003), New directions: Atmospheric brown "clouds", *Atmos. Environ.*, *37*(28), 4033–4035.

Ramanathan, V., et al. (2007), Atmospheric brown clouds: Hemispherical and regional variations in long-range transport, absorption, and radiative forcing, *J. Geophys. Res.*, *112*, D22S21, doi:10.1029/2006JD008124.

Rastogi, N., and M. M. Sarin (2005), Long-term characterization of ionic species in aerosols from urban and high-altitude sites in western India: Role of mineral dust and anthropogenic sources, *Atmos. Environ.*, *39*(30), 5541–5554.

Rastogi, N., and M. M. Sarin (2009), Quantitative chemical composition and characteristics of aerosols over western India: One-year record of temporal variability, *Atmos. Environ.*, *43*(22–23), 3481–3488.

Reff, A., S. I. Eberly, and P. V. Bhave (2007), Receptor modeling of ambient particulate matter data using positive matrix factorization: Review of existing methods, *J. Air Waste Manage. Assoc.*, *57*(2), 146–154.

Remer, L. A., et al. (2005), The MODIS aerosol algorithm, products and validation, *J. Atmos. Sci.*, *62*, 947–973.

Rengarajan, R., M. M. Sarin, and A. K. Sudheer (2007), Carbonaceous and inorganic species in atmospheric aerosols during wintertime over urban and high-altitude sites in North India, *J. Geophys. Res.*, *112*, D21307, doi:10.1029/2006JD008150.

Shen, Z. X., J. J. Cao, R. Arimoto, R. J. Zhang, D. M. Jie, S. X. Liu, and C. S. Zhu (2007), Chemical composition and source characterization of spring aerosol over Horqin sand land in northeastern China, *J. Geophys. Res.*, *112*, D14315, doi:10.1029/2006JD007991.

Shen, Z. X., J. J. Cao, R. Arimoto, Z. W. Han, R. J. Zhang, Y. M. Han, S. X. Liu, T. Okuda, S. Nakao, and S. Tanaka (2009), Ionic composition of TSP and $PM_{2.5}$ during dust storms and air pollution episodes at Xi'an, China, *Atmos. Environ.*, *43*(18), 2911–2918.

Shrestha, A. B., C. P. Wake, J. E. Dibb, P. A. Mayewski, S. I. Whitlow, G. R. Carmichael, and M. Ferm (2000), Seasonal variations in aerosol concentrations and compositions in the Nepal Himalaya, *Atmos. Environ.*, *34*(20), 3349–3363.

Tang, J., X. L. Yu and H. S. Xue (2005), Observation of the water-soluble species in aerosols in summer in Lhasa area: Contribution of biomass burning emission, Paper presented at eighth symposium on aerosol research and aerosol technology in China and cross the Taiwan Strait, pp. 355, Nanjing, China. (in Chinese).

Tang, M. (1998), *Formation, Evolution and Variability Characteristics of Qinghai-Tibetan Plateau Monsoon*, Guangdong Sciences and Technology Press, Guangzhou, pp. 161–182.

Torres, O., A. Tanskanen, B. Veihelmann, C. Ahn, R. Braak, P. K. Bhartia, P. Veefkind, and P. Levelt (2007), Aerosols and surface UV products from ozone monitoring instrument observations: An overview, *J. Geophys. Res.*, *112*, D24S47, doi:10.1029/2007JD008809.

Turpin, B. J., and H.-J. Lim (2001), Species contributions to $PM_{2.5}$ mass concentrations: Revisiting common assumptions for estimating organic mass, *Aerosol Sci. Tech.*, *35*(1), 602–610.

Venkataraman, C., C. K. Reddy, S. Josson, and M. S. Reddy (2002), Aerosol size and chemical characteristics at Mumbai, India, during the INDOEX-IFP (1999), *Atmos. Environ.*, *36*(12), 1979–1991.

Venzac, H., et al. (2008), High frequency new particle formation in the Himalayas, *Proc. Natl. Acad. Sci. U. S. A.*, *105*(41), 15,666–15,671.

Watson, J. G., T. Zhu, J. C. Chow, J. P. Engelbrecht, E. M. Fujita, W. E. Wilson (2002), Receptor modeling application framework for particle source apportionment, *Chemosphere*, *49*(9), 1093–1136.

Wen, Y. P., X. B. Xu, J. Tang, X. C. Zhang, and Y. C. Zhang (2001), Enrichment characteristics and origin of atmospheric aerosol elemental at Mt. Waliguan, *J. Appl. Meteorol. Sci.*, *12*(4), 400–408 (in Chinese).

Wu, G. X., Y. M. Liu, T. M. Wang, R. J. Wan, X. Liu, W. P. Li, Z. Z. Wang, Q. Zhang, A. M. Duan, and X. Y. Liang (2007), The influence of mechanical and thermal forcing by the Tibetan plateau on Asian climate, *J. Hydrometeorol.*, *8*(4), 770–789.

Xia, X. A., X. M. Zong, Z. Y. Cong, H. B. Chen, S. C. Kang, and P. C. Wang (2011), Baseline continental aerosol over the central Tibetan plateau and a case study of aerosol transport from South Asia, *Atmos. Environ.*, *45*(39), 7370–7378.

Xia X. A., P. C. Wang, Y. S. Wang, Z. Q. Li, J. Y. Xin, J. Liu and H. B. Chen (2008), Aerosol optical depth over the Tibetan plateau and its relation to aerosols over the Taklimakan Desert, *Geophys. Res. Lett.*, *35*, L16804, doi:10.1029/2008GL034981.

Xu, B. Q., et al. (2009), Black soot and the survival of Tibetan glaciers, *Proc. Natl. Acad. Sci. U. S. A.*, *106*(52), 22,114–22,118.

Xu, H. M., et al. (2012), Lead concentrations in fine particulate matter after the phasing out of leaded gasoline in Xi'an, China, *Atmos. Environ.*, *46*, 217–224.

Xu, J., M. H. Bergin, R. Greenwald, J. J. Schauer, M. M. Shafer, J. L. Jaffrezo, and G. Aymoz (2004), Aerosol chemical, physical, and radiative characteristics near a desert source region of northwest China during ACE-Asia, *J. Geophys. Res.*, *109*, D19S03, doi:10.1029/2003JD004239.

Zhang, T., et al. (2011), Water-soluble ions in atmospheric aerosols measured in Xi'an, China: Seasonal variations and sources, *Atmos. Res.*, *102*(1–2), 110–119.

Zhang, X. Y., S. L. Gong, R. Arimoto, Z. X. Shen, F. M. Mei, D. Wang, and Y. Cheng (2003), Characterization and temporal variation of Asian dust aerosol from a site in the Northern Chinese deserts, *J. Atmos. Chem.*, *44*(3), 241–257.